Normal and anomalous diffusion in a bouncing ball over an irregular surface

Ana Laura Boscolo, Valdir Barbosa da Silva Junior, and Luiz Antonio Barreiro *
Institute of Geosciences and Exact Sciences, Physics Department, São Paulo State University (Unesp), CEP 13506-900, Rio Claro, São Paulo, Brazil

(Received 6 January 2023; accepted 22 March 2023; published 18 April 2023)

The problem of a bouncing ball on a nonplanar surface is investigated. We discovered that surface undulation adds a horizontal component to the impact force, which acquires a random character. Some aspects of Brownian motion are found in the horizontal distribution of the particle. On the x axis, normal and superdiffusion are observed. For the probability density's functional form, a scaling hypothesis is presented.

DOI: 10.1103/PhysRevE.107.045001

I. INTRODUCTION

Diffusion is a common natural phenomenon and generally occurs when a system moves toward the equilibrium state [1]. Many domains employ the notion of diffusion, including physics (particle diffusion), chemistry, biology, sociology, economics, and finance [2–4]. They all represent the fundamental concept of diffusion, which asserts that a substance or collection expands away from a point or location where that material or collection is more concentrated. In a diffusion process in a set of moving elements—energy, linear momentum, atoms, molecules, cells, animals, etc.—each element performs a random trajectory. As a result of this highly irregular individual movement, the ensemble diffuses. Many nonlinear systems also present a diffusive behavior in your phase space. Modeling such a dynamic system has become one of the most challenging subjects among scientists. The modeling helps to understand in many cases how the system evolves in time [5–7].

On a macroscopic level, the average collective behavior, in contrast to the microscopic individual movement, shows great regularity and follows well-defined dynamic laws. The nonlinear dynamic formulation of these transport phenomena, as well as the diffusion equation, are two ways to describe the diffusion phenomena. The form of the temporal dependence of the mean-squared distance (MSD), $\langle x^2\rangle \propto t^{2\mu}$, or, equivalently, of the variance, allows classifying the type of diffusion. For $\mu = 1/2$ we have the usual or normal diffusion, which can be described by Fick's laws. Otherwise, we have an anomalous diffusion (or non-Fickian diffusion). When $\mu > 1/2$ the case is classified as superdiffusive [8,9] and for $\mu < 1/2$ we have the subdiffusive case [10,11]. Indeed, a wide diversity of systems presents a nonlinear growth of the mean-squared displacement.

In this work, we explore the diffusive behavior that occurs in a free-falling particle colliding with a nonplanar surface. Compared to a flat surface, on which the falling particles maintain their velocity in the horizontal direction, a nonplanar surface introduces changes in the horizontal component of velocity after each collision. This creates a spread in the absolute value of the horizontal component of velocity as well as in its signal. Thus, in Sec. II we study the dynamics of the model, in which the equations of motion are established, and how the iterative process takes place. Some special points are explored in Sec. II C, for which no diffusion is observed. In Sec. III, the randomness of the horizontal component of the collision force is studied. Also, the diffusion in the signal of the horizontal component of velocity and its relation to the random walk problem are explored. Section IV is devoted to discussing the behavior of the mean-squared displacement in relation to the initial collision point and the probability distribution function (PDF) numerically and analytically. In Sec. V, the conclusions and final considerations about the problem addressed are presented.

II. THE MODEL

We now discuss how to construct the equations of the mapping that describe the dynamics of the particles. The model under study consists of an ensemble of noninteracting classical particles of mass m traveling in the presence of a constant gravitational field $\boldsymbol{g}$ and colliding with a nonflat ground via elastic collisions. The parametric equations that describe the ground are

$$\begin{aligned} x(p) &= \alpha p, \\ y(p) &= \beta[1+\cos(p)]. \end{aligned} \tag{1}$$

Figure 1 shows an example with $\alpha = 0.01$ and $\beta = 0.005$. Here it is worth noting that if the β parameter is null, then the floor becomes flat, recovering the traditional bouncer model [12] with a static floor. However, different from the traditional bouncer model, if $\beta \neq 0$, the particles gain an extra degree of freedom, with movement in the x direction too. Also, as in the bouncer model, the action of the constant gravitational field g is responsible for the return mechanism of the particle for the next collision with the floor. The conservation of energy during the collision is controlled by a parameter which is called the *coefficient of restitution* and it is denoted by γ. For $\gamma = 1$ the conservative dynamics is observed. However, if $0 < \gamma < 1$ we found a dissipative behavior. A model similar

*luiz.a.barreiro@unesp.br

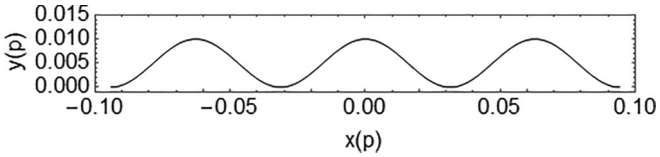

FIG. 1. Graph obtained from Eqs. (1) using the parameters $\alpha = 0.01$ and $\beta = 0.005$.

to the one described in this paper was investigated in Ref. [13] to explain how anomalous diffusion happens as a result of orbital stickiness to islands of stability.

A. The map

We now explore the time evolution of particles, determining the coordinates of the collision points and their respective velocities. The dynamic evolution of the particle can be described by Newton's equation of motion

$$m\frac{d\boldsymbol{v}}{dt} = \boldsymbol{F}_{\text{grav}} + \boldsymbol{F}_{\text{col}}, \tag{2}$$

where $\boldsymbol{F}_{\text{grav}} = m\boldsymbol{g}$ is the gravitational force acting on the particle and $\boldsymbol{F}_{\text{col}}$ represents the instantaneous force of collision with the ground. We will assume that the collision force only changes the velocity component orthogonal to the surface. It is also an acceptable assumption that during the collision process the force $\boldsymbol{F}_{\text{col}}$ has an extremely rapid variation.

A typical path taken by the particles is shown in Fig. 2. After the nth collision at the point defined by the parameter p_n, the particle travels in the gravitational field until it collides at the point p_{n+1}. This journey takes a $\delta t_{n,n+1}$ time and continues incessantly if no dissipation is taken into account. The normal vectors at each collision point are also shown. The unit normal and tangent vectors at the point p_n can be written in terms of the Cartesian vectors as

$$\hat{\boldsymbol{n}}_n = \frac{(-\lambda_n\,\boldsymbol{i} + \boldsymbol{j})}{\sqrt{1+\lambda_n^2}} \quad \text{and} \quad \hat{\boldsymbol{t}}_n = \frac{(\boldsymbol{i} + \lambda_n\,\boldsymbol{j})}{\sqrt{1+\lambda_n^2}}, \tag{3}$$

where λ_n is the local inclination of the ground, which for the functions in (1), is given by

$$\lambda_n = \frac{(dy/dp)_{p_n}}{(dx/dp)_{p_n}} = -\frac{\beta}{\alpha}\sin(p_n). \tag{4}$$

Since motion in the gravitational field is a well-known problem, the fundamental question in determining the dynamic evolution of the particle will be to find the points of collision with the ground. To proceed with this determination,

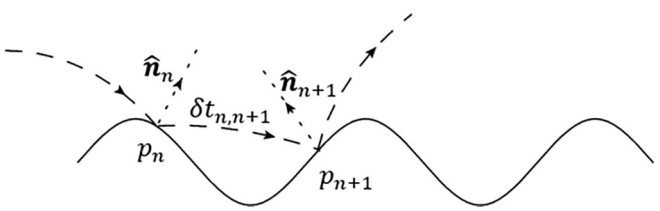

FIG. 2. Schematic drawing of the trajectory of a particle, with its collision points and the respective normal vectors.

we define the following two functions:

$$\begin{aligned} G_X(p,t) &= x(p) - \left[x(p_n) + v_{x_n}^{(r)}t\right], \\ G_Y(p,t) &= y(p) - \left[y(p_n) + v_{y_n}^{(r)}t - \frac{g}{2}t^2\right], \end{aligned} \tag{5}$$

where $(v_{x_n}^{(r)}, v_{y_n}^{(r)})$ is the velocity of the particle after it collides at point p_n. The next point p_{n+1} and the travel time $\delta t_{n,n+1} = (t_{n+1} - t_n)$ spent by the particle between p_n and p_{n+1} are obtained by solving the system of transcendental equations

$$\begin{aligned} G_X(p_{n+1}, \delta t_{n,n+1}) &= 0, \\ G_Y(p_{n+1}, \delta t_{n,n+1}) &= 0. \end{aligned} \tag{6}$$

In such a way, if the particles make a trip with N collisions, the total time spent will be

$$t_N = \sum_{n=1}^{N} \delta t_{n-1,n} \quad \text{with } t_0 = 0. \tag{7}$$

In our model, we assume that only the component of the velocity normal to the surface at the collision point is altered (inverted) [14]. Then, at the instant of collision, the law of reflection relating the incident velocity vector $\boldsymbol{v}_n^{(i)}$ to the reflected velocity vector $\boldsymbol{v}_n^{(r)}$ is

$$\boldsymbol{v}_n^{(r)} = \left(\boldsymbol{v}_n^{(i)} \cdot \hat{\boldsymbol{t}}_n\right)\hat{\boldsymbol{t}}_n - \gamma_n\left(\boldsymbol{v}_n^{(i)} \cdot \hat{\boldsymbol{n}}_n\right)\hat{\boldsymbol{n}}_n. \tag{8}$$

Obviously, the velocity vector, incident at a point p_{n+1}, is related to the velocity vector reflected at the previous point p_n as

$$\boldsymbol{v}_{n+1}^{(i)} = v_{x_n}^{(r)}\boldsymbol{i} + \left(v_{y_n}^{(r)} - g\,\delta t_{n,n+1}\right)\boldsymbol{j}.$$

Now we can define the following dimensionless variables $\bar{x}(p) = x(p)/gt_N^2$, $\bar{y}(p) = y(p)/gt_N^2$, $\bar{\boldsymbol{v}}_n^{(r)} = \boldsymbol{v}_n^{(r)}/gt_N$, and $\phi_n = t_n/t_N$, where t_N is defined in (7). Therefore, the compact time $\phi \in [0, 1]$ and the dimensionless velocity vector components in (8) take the form

$$\begin{aligned} \bar{v}_{x_{n+1}}^{(r)} &= \frac{\left(1-\gamma_{n+1}\lambda_{n+1}^2\right)\bar{v}_{x_n}^{(r)} + \lambda_{n+1}(1+\gamma_{n+1})\left(\bar{v}_{y_n}^{(r)} - \delta\phi_{n,n+1}\right)}{1+\lambda_{n+1}^2}, \\ \bar{v}_{y_{n+1}}^{(r)} &= \frac{\lambda_{n+1}(1+\gamma_{n+1})\bar{v}_{x_n}^{(r)} + \left(\lambda_{n+1}^2 - \gamma_{n+1}\right)\left(\bar{v}_{y_n}^{(r)} - \delta\phi_{n,n+1}\right)}{1+\lambda_{n+1}^2}. \end{aligned} \tag{9}$$

So the system (6) becomes

$$\begin{aligned} p_{n+1} &= p_n + \frac{\bar{v}_{x_n}^{(r)}}{\bar{\alpha}}\delta\phi_{n,n+1}, \\ \cos(p_{n+1}) &= \cos(p_n) + \frac{\bar{v}_{y_n}^{(r)}}{\bar{\beta}}\delta\phi_{n,n+1} - \frac{1}{2\bar{\beta}}\delta\phi_{n,n+1}^2, \end{aligned} \tag{10}$$

where $\bar{\alpha} = \alpha/gt_N^2$ and $\bar{\beta} = \beta/gt_N^2$. Given the values of p_n, $\bar{v}_{x_n}^{(r)}$, and $\bar{v}_{y_n}^{(r)}$ of the nth iteration, the set of equations (10) produce the values of p_{n+1} and the travel time $\delta\phi_{n,n+1}$ which allows us to find $\bar{v}_{x_{n+1}}^{(r)}$ and $\bar{v}_{y_{n+1}}^{(r)}$ through (9). After that, the iterative process restarts.

B. Conservative case

We shall only consider the conservative scenario, when $\gamma_n = \gamma_{n+1} = 1$. Since we choose $\bar{\beta} \ll 1$, it is appropriate to

consider that the point of collision with the ground has a height $\bar{y}(p_n) \simeq \bar{y}(p_{n+1}) \simeq 0$, but with local slope not necessarily zero. This approach avoids transcendental equations and simplifies the calculation. As a consequence, the second of the equations in (10) yields $\delta\phi_{n,n+1} = \phi_{n,n+1} - \phi_n = 2\bar{v}_{y_n}^{(r)}$. Finally, a simplified form of the map equations used to explain motion is expressed as

$$\bar{v}_{x_{n+1}}^{(r)} = F_1\left(\bar{v}_{x_n}^{(r)}, \bar{v}_{y_n}^{(r)}, p_n\right), \tag{11a}$$

$$\bar{v}_{y_{n+1}}^{(r)} = \left|F_2\left(\bar{v}_{x_n}^{(r)}, \bar{v}_{y_n}^{(r)}, p_n\right)\right|, \tag{11b}$$

$$p_{n+1} = F_3\left(\bar{v}_{x_n}^{(r)}, \bar{v}_{y_n}^{(r)}, p_n\right), \tag{11c}$$

where

$$F_1\left(\bar{v}_{x_n}^{(r)}, \bar{v}_{y_n}^{(r)}, p_n\right) = \frac{\left(1-\bar{\lambda}_n^2\right)\bar{v}_{x_n}^{(r)} - 2\bar{\lambda}_n\bar{v}_{y_n}^{(r)}}{1+\bar{\lambda}_n^2}, \tag{12a}$$

$$F_2\left(\bar{v}_{x_n}^{(r)}, \bar{v}_{y_n}^{(r)}, p_n\right) = \frac{2\bar{\lambda}_n\bar{v}_{x_n}^{(r)} + \left(1-\bar{\lambda}_n^2\right)\bar{v}_{y_n}^{(r)}}{1+\bar{\lambda}_n^2}, \tag{12b}$$

$$F_3\left(\bar{v}_{x_n}^{(r)}, \bar{v}_{y_n}^{(r)}, p_n\right) = p_n + \frac{2}{\alpha}\bar{v}_{x_n}^{(r)}\bar{v}_{y_n}^{(r)}, \tag{12c}$$

and were defined as

$$\bar{\lambda}_n = \lambda_{n+1} = -\frac{\bar{\beta}}{\bar{\alpha}}\sin\left(p_n + \frac{2}{\alpha}\bar{v}_{x_n}^{(r)}\bar{v}_{y_n}^{(r)}\right). \tag{13}$$

The ground was assumed to be flat; as a consequence there is a possibility that $\bar{v}_{y_{n+1}}^{(r)} = F_2 < 0$. This nonphysical situation is bypassed by introducing the modulus in Eq. (11b). This means that if such a case happens, the particle is reinjected back to the dynamics with the same velocity but with a positive direction. The system stays conservative with the flat floor approximation, as proven by finding the determinant of the Jacobian matrix for this system and ensuring that it equals 1. Mathematical details are presented in the Appendix.

C. Periodic orbits

We can anticipate the occurrence of some exceptional points using the physics of the problem. These are known as fixed points, to which the dynamical system returns after one iteration (period-one orbit), two iterations (period-two orbit), or n iterations (period-n orbit). Figure 3 illustrates two fixed points: (a) period-one and (b) period-two orbits.

1. Period-one orbit

It is evident that period-one orbits, as shown in portion (a) of Fig. 3, have a zero local slope. So, as long as the x component of the initial velocity is zero, the system will not experience any diffusion in the horizontal axis. A period-one orbit is obtained by solving the following equations: $\bar{v}_{x_{n+1}}^{(r)} = \bar{v}_{x_n}^{(r)} = 0$, $\bar{v}_{y_{n+1}}^{(r)} = \bar{v}_{y_n}^{(r)}$, and $p_{n+1} = p_n$ with $\bar{\lambda}_n = 0$ (zero slope). We can verify the fact considering the first equation in (13)

$$\bar{\lambda}_n = 0 \Rightarrow \sin\left(p_n + \frac{2}{\alpha}\bar{v}_{x_n}^{(r)}\bar{v}_{y_n}^{(r)}\right) = 0 \underset{\bar{v}_{x_n}^{(r)}=0}{\Rightarrow} p_n = m\pi,$$

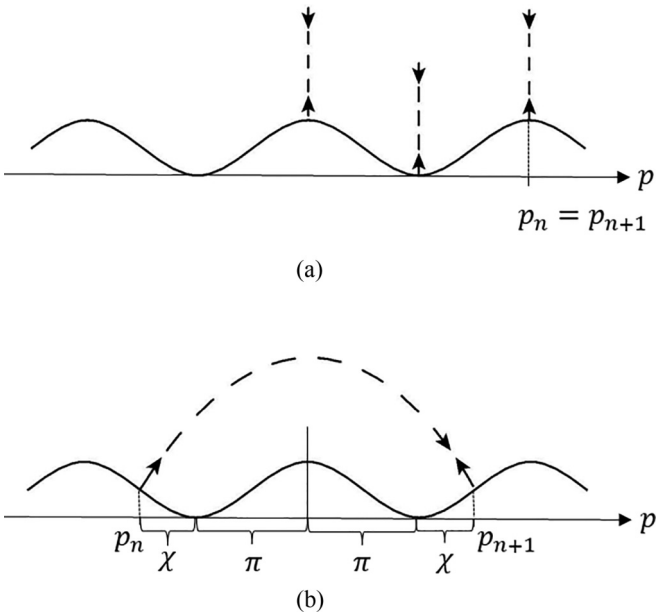

FIG. 3. Examples of periodic orbits: (a) period-one orbit. The dynamical system returns to the point in phase space at each iteration and (b) period-two orbit when the system returns to the point after two iterations.

where m is an integer. These points indicate the locations of the peaks and valleys in Fig. 3(a). Thus

$$\begin{aligned}\bar{v}_{x_{n+1}}^{(r)} &= F_1\left(0, \bar{v}_{y_n}^{(r)}, m\pi\right) = 0,\\ \bar{v}_{y_{n+1}}^{(r)} &= F_2\left(0, \bar{v}_{y_n}^{(r)}, m\pi\right) = \bar{v}_{y_n}^{(r)},\\ p_{n+1} &= F_3\left(0, \bar{v}_{y_n}^{(r)}, m\pi\right) = m\pi.\end{aligned} \tag{14}$$

We have the following physical situation: If a particle is chosen whose horizontal component of velocity is zero, in a zero slope point, clearly the x coordinate of the particle will never change and the particle does not scatter in the x direction.

2. Period-two orbits

We now consider points with nonzero slope. In general, the particle gains a nonzero horizontal component to the velocity and then diffuses along the horizontal axis. Nevertheless, depending on the initial conditions, it is possible for the particle to strike the surface at point p_n with velocity $\vec{v}_n$, reflect there, then it reaches point p_{n+1} with velocity $\vec{v}_{n+1}$, where it will then reflect again and go back to point p_n with velocity $\vec{v}_n$. Figure 3(b) depicts an illustration of this kind. Inspired by the figure, consider points connected by $\bar{v}_{x_{n+2}}^{(r)} = -\bar{v}_{x_{n+1}}^{(r)} = \bar{v}_{x_n}^{(r)}$, $\bar{v}_{y_{n+2}}^{(r)} = \bar{v}_{y_{n+1}}^{(r)} = \bar{v}_{y_n}^{(r)}$, $p_{n+2} = p_n$, $\bar{y}(p_{n+1}) = \bar{y}(p_n)$, and opposite local slopes $\bar{\lambda}_{n+1} = -\bar{\lambda}_n$.

Taking into account Fig. 3(b), the points p_n and p_{n+1} must be connected by

$$\begin{cases} p_n = -\pi - \chi \\ p_{n+1} = \pi + \chi \end{cases} \text{with } 0 < \chi < \pi,$$

where we are solely concerned with the most straightforward solution. Then, with the help of Eqs. (10), we can write

$$\bar{v}_{x_n}^{(r)}\bar{v}_{y_n}^{(r)} = \bar{\alpha}(\pi + \chi). \tag{15}$$

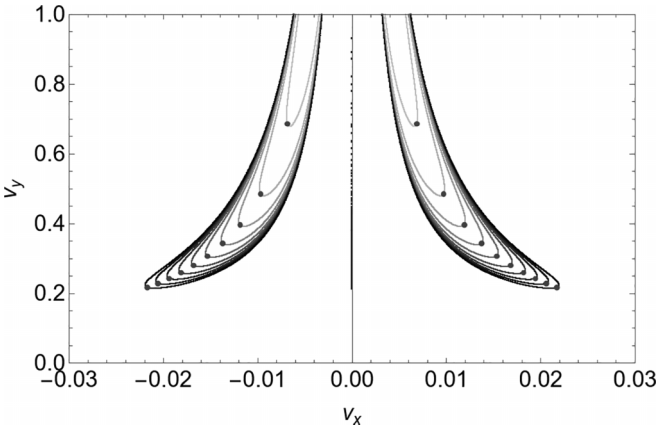

FIG. 4. Period-one orbits are represented by the black dots in the center of the line. The other points are the period-two orbits.The gray dots at the end of the curves are the points obtained with the value $\chi = \pi/2$.

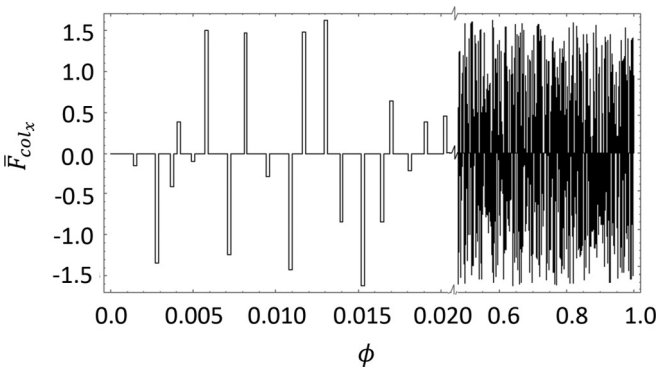

FIG. 5. Typical behavior of the horizontal component of the collision force $\bar{F}_{\mathrm{col}_x}$. Here we have used $\bar{\alpha} = 0.01$ and $\bar{\beta} = 0.005$. The graph has two regions with different scales. On the left we have the region magnified between $\phi = 0.000$ and $\phi = 0.020$ and on the right, after a cut in the graph, the normal scale from $\phi = 0.5$ to $\phi = 1.0$ is shown.

In addition, the first of Eqs. (12b) yields

$$\bar{v}_{y_n}^{(r)} = \frac{\bar{\alpha}}{\bar{\beta}\sin(\chi)}\bar{v}_{x_n}^{(r)}. \tag{16}$$

These results allow us to determine both $\bar{v}_{x_n}^{(r)}$ and $\bar{v}_{y_n}^{(r)}$ as functions of χ. So the points for period-two orbits are written as

$$\bar{v}_{x_n}^{(r)} = \pm\sqrt{\bar{\beta}(\pi+\chi)\sin(\chi)},$$
$$\bar{v}_{y_n}^{(r)} = \frac{\bar{\alpha}(\pi+\chi)}{\sqrt{\bar{\beta}(\pi+\chi)\sin(\chi)}},$$
$$p_n = \mp(\pi+\chi).$$

Figure 4 illustrates these points. The middle points in black in this picture indicate the period-one orbit. The graphic also illustrates the effect of the β parameter on the formation of period-two orbits. The points are calculated by altering the value of χ from 0 to π, and each gray level indicates a β parameter value from the lightest gray ($\beta = 0.000\,01$) to the darkest ($\beta = 0.0001$). $\alpha = 0.001$ is used for all points.

The choice $\chi = \pi/2$ is used to calculate the gray dots in Fig. 4. Each curve is divided into two branches by these points. The points that make up the branches we name external have $\chi > \pi/2$, whereas the points that make up the branches we term internal have $\chi < \pi/2$. Consider the eigenvalues of the Jacobian matrix to categorize the stability of these points. The external points ($\chi \geqslant \pi/2$) can be classified as node-type stable points since the modules of their Jacobian matrix eigenvalues are all equal to 1. On the other hand, because all of the eigenvalues are real with one positive and the others negatives, the internal points ($\chi < \pi/2$) are categorized as unstable points of the saddle type. Therefore, the gray dots in the phase space represent saddle-node bifurcations [15].

Many more types of fixed points may exist, and this subject will be addressed in future work. We are mostly interested in the particle dispersion problem along the horizontal axis in this work.

III. DIFFUSION PROCESS

A. The stochastic character of force

Clearly, unless we are in some special initial point, the particles must diffuse in the x direction. This diffusion is caused by the collision force with the ground. Due to the irregular nature of the ground, the collision force $\boldsymbol{F}_{\mathrm{col}}$ has components in both horizontal and vertical directions. It is intuitive to notice that the horizontal component presents different magnitudes and directions at each collision. To understand the behavior of this horizontal component of the collision force, we can describe it as

$$\bar{F}_{\mathrm{col}_x}(\phi_n) = \left.\frac{\Delta\bar{v}}{\bar{\tau}}\right|_{p_n} = \frac{\bar{v}_{x_n}^{(r)} - \bar{v}_{x_n}^{(i)}}{\bar{\tau}} = \frac{\bar{v}_{x_n}^{(r)} - \bar{v}_{x_{n-1}}^{(r)}}{\bar{\tau}},$$

where $\bar{\tau}$ is the dimensionless collision time, which is extremely small. We will also assume that the collision force is approximately constant during the collision time and a typical example of what this force looks like is shown in Fig. 5.

The width of each rectangle represents the collision time and despite the dynamics being well known and the irregularities in the ground having a periodicity, the numerical results presented show that the effects of the horizontal component of this force has a behavior comparable to a stochastic force. It is actually extremely difficult to tell whether a sequence is random or chaotic, but there are some proposed procedures to distinguish between these two behaviors. In this work we will make use of the permutation entropy (PE) method [16,17] to establish the randomness of the time series produced by the collision force. Denoting the time series as $\{S_t\}_{t=1,\ldots,T}$ the method consists in defining subsets of order O, forming the set $S = \{\{S_1, S_2, \ldots, S_O\}, \{S_2, S_3, \ldots, S_{O+1}\}, \ldots, \{S_{T-O+1}, \ldots, S_{T-1}, S_T\}\}$. We then compare consecutive values from each subset to establish the associated permutation. For example, $\{S_1 < S_2 < \cdots < S_O\}$ represents the permutation $\{1, 2, \ldots., O\}$, while $\{S_2 < S_1 < \cdots < S_O\}$ represents the permutation $2, 1 \ldots, O$ and so on, yielding the set of all permutations associated with the sequence S, named $\Pi(S)$. Then, the set of all $O!$ possible permutations π_i of the numbers $\{1, 2, \ldots, O\}$ are constructed.

TABLE I. The initial conditions are chosen in order to vary the initial point $[x(p_0), y(p_0)]$ and keeping the energy $\bar{E} = 4$ constant.

Floor parameters	Initial condition	$O = 3$	$O = 4$	$O = 5$	$O = 6$
$\alpha = 0.01$	$p_0 = -0.033$	0.998569	0.995189	0.981222	0.92671
$\beta = 0.005$	$p_0 = 0.032$	0.999633	0.995120	0.982245	0.925946
$\alpha = 0.01$	$p_0 = -0.033$	0.998874	0.994082	0.986440	0.935262
$\beta = 0.0005$	$p_0 = 0.032$	0.999501	0.996295	0.984878	0.934281

The relative frequency of each permutation π_i can be calculated by counting the number of times the permutation π_i is found in the set $\Pi(S)$ divided by the total number of sequences,

$$P_i = \frac{\text{Number of times that } \pi_i \text{ appears in } \Pi(S)}{T - O + 1}, \tag{17}$$

and the normalized permutation entropy function is written as

$$\text{PE}_O = -\frac{1}{\log_2(O!)} \sum_{i=1}^{O!} P_i \log_2(P_i). \tag{18}$$

Formulas (17) and (18) were applied to the temporal sequences of collision forces for three different initial conditions and also different orders O. Table I shows the results obtained. The smaller the PE_O, the more regular and more deterministic the time series. Contrarily, the closer to 1 the value of PE_O, the more noisy and random the time series. The results allow us to assume that the force is random.

IV. PDF

This section's major purpose is to establish the PDF $\Psi(x, t)$, which provides us the probability of the particle being on the coordinate x at time t, and what it has to do with normal and superdiffusive processes. Among the various diffusive processes, Brownian motion is the prototype for the description of nonequilibrium dynamical systems. Due to the stochastic behavior of the collision force, the jumps performed by the particles also reproduce characteristics of random walk. We can comprehend this by calculating the chance of each particle going to the right. After each impact, we obtain the x component of the velocity. Then, by examining the sign of these velocities and associating $+1$ for $v_x > 0$ and 0 for $v_x < 0$, we can count the number of jumps to the right and derive the evolution of this probability as the number of jumps increases. It is appropriate at this point to introduce an index that specifies the initial condition (ν), which is used to compute the PDF for the complete ensemble. So, starting with an initial state labeled by ν, the probability of jumping to the right after n jumps is calculated as follows:

$$P_{r\ \text{jump}}(n, \nu) = \frac{1}{n} \sum_{i=1}^{n} \text{SgnPlus}\left(v_{x,i}^{(\nu)}\right),$$

$$\text{where} \quad \text{SgnPlus}(v_x) = \begin{cases} 1 & \text{if } v_x > 0 \\ 0 & \text{if } v_x < 0. \end{cases}$$

Figure 6, on the left, shows examples of the time progression of individual particle jumps for four distinct initial conditions and two ground parameter adjustments, as well as the corresponding PDFs $\Psi(\bar{x}, \phi)$. With time evolution, the left and right jump probabilities for a ground with $\bar{\alpha} = 0.01$ and $\bar{\beta} = 0.005$ tend to be 0.5 very quickly as we can see in the upper graphic on the left. However, if the β parameter is set to $\bar{\beta} = 0.0005$ the graph indicates an initial oscillation, but the probability ultimately tends to reach 0.5.

The coordinates of the collision points and the travel time between one point and the next are obtained from the mapping given in Eqs. (9) and (10). It is obvious that the travel time varies between jumps. However, for our analysis, it is critical to obtain the particle's position as a function of time with equal time intervals. This is simple because the particle moves in a gravitational field $\boldsymbol{g}$, and we can easily calculate its position as a function of time. The time is then normalized so that the maximum time equals 1. So, to get the probability distribution, for all iterative processes, we begin by subtracting the starting position of the particles. As a result, all of the particles in the ensemble start from the same position. In our scenario, we have 2000 particles performing 4000 leaps, totaling 8×10^6 collision points, but it is clear that the number of points as a function of time depends on the choice of interval dt and can be much higher. To demonstrate the procedure, the simulation is configured so that each particle in the ensemble has an energy of $\bar{E} = 4$. The outcomes for two different types of grounds are shown in Fig. 6 on the right.

The first PDF graph was obtained with the parameters $\bar{\alpha} = 0.01$ and $\bar{\beta} = 0.005$, and shows a probability density region following a format very similar to a Gaussian distribution. The second PDF, obtained with the parameters $\bar{\alpha} = 0.01$ and $\bar{\beta} = 0.0005$, has an extremely anomalous diffusion in the early part of its time evolution; however, when the time evolution takes place, the PDF apparently starts to show a Gaussian behavior. In order to have a better understanding of this behavior, we studied the moments associated with each distribution. Inspired by the Gaussian form of normal diffusion, with an anomalous diffusion we make a scaling hypothesis [18] so that we can express the anomalous distribution as

$$\Psi_\mu(\bar{x}, \phi) = \sqrt{\frac{a}{\pi}} \frac{1}{\phi^\mu} \exp\left[-a\left(\frac{\bar{x}}{\phi^\mu}\right)^2\right]. \tag{19}$$

It should be noted at this point that when we make the Gaussian hypothesis, Eq. (19), we are implicitly assuming that the force depicted in Fig. 5 is related to Mandelbrot's theory of fractional Brownian motion (FBM) [19]. Like the authors of Ref. [18], we do not intend to provide a theoretical derivation of the FBM. Obtaining the Gaussian form (19), as well as its parameters, from the FBM described in Fig. 5 is, in fact, a significant theoretical open problem. Instead of addressing this issue directly, we deal with the moments associated with

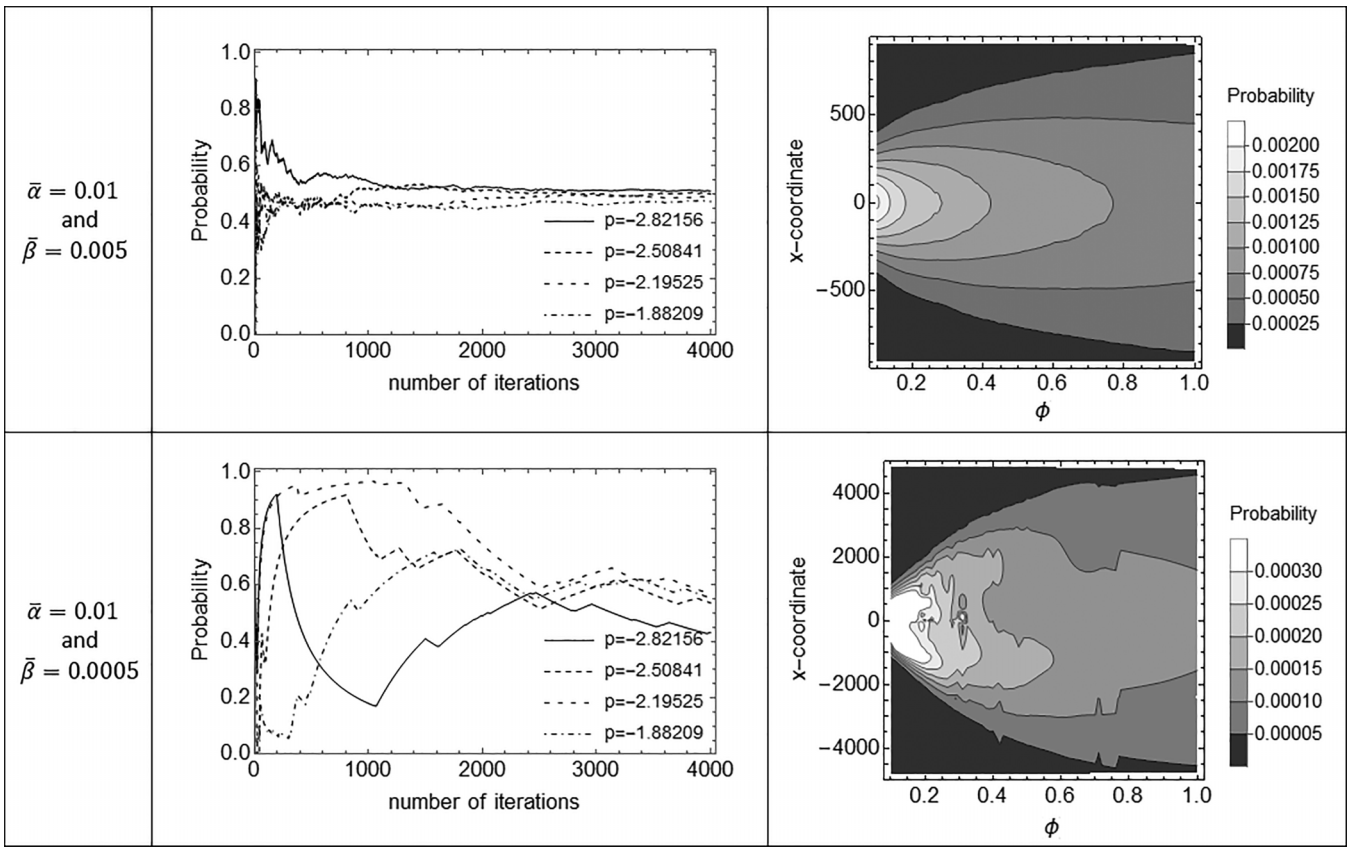

FIG. 6. The first graphic of each column contains time evolution examples for the likelihood of a single particle jumping to the right. The difference is in the β parameter value, which is lowered to one-tenth and one-hundredth of its initial value in the columns on the left. The evolution of the four-particle leaps (four initial conditions) is explored in the graphs. The different initial conditions for the particles are obtained by changing the initial parameter p in the functions $x(p)$ and $y(p)$ in Eq. (1) and keeping the energy $\bar{E} = 4$ constant. The selected p parameters are shown in the figures. The respective contour plots for the probability distributions are shown on the right.

the distribution which can be easily derived as

$$\langle|\bar{x}(\phi)|^m\rangle = \int_{-\infty}^{\infty} \bar{x}^m \Psi_\mu(\bar{x},\phi)\, d\bar{x} = \frac{1}{\sqrt{a^m \pi}} \Gamma\left(\frac{m+1}{2}\right) \phi^{m\mu}. \tag{20}$$

The result shows a behavior of MSD as $\langle \bar{x}^2 \rangle \propto \phi^{2\mu}$, therefore normal distribution has a scale parameter $\mu = 1/2$. If $\mu < 1/2$ we have a subdiffusive process and for $\mu > 1/2$ we found a superdiffusive behavior. Fure 7 shows the results of the moments calculations for two different grounds. We

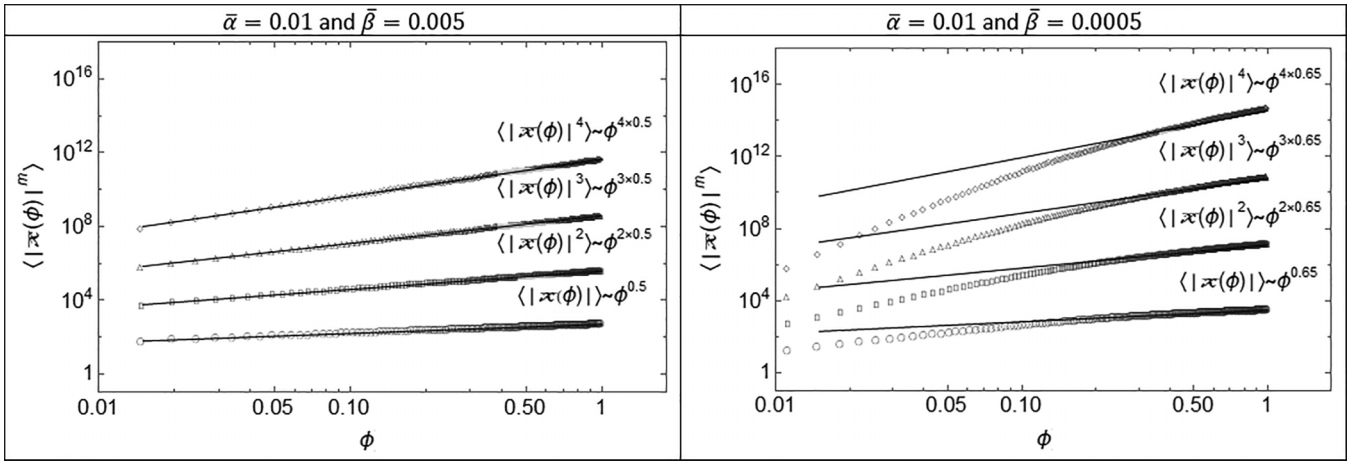

FIG. 7. The black lines represent equations of powers $\phi^{m\mu}$. At left we have a normal diffusion and at right we have a superdiffusive process. We can see that more than half of the time evolution has passed before the superdiffusive behavior with scale $\mu = 0.65$ manifests.

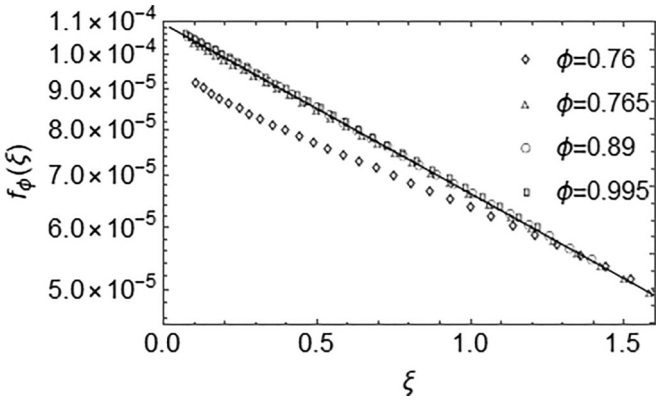

FIG. 8. PDFs rescaled by the factor $\xi = \bar{x}^2/\langle \bar{x}(\phi)^2 \rangle$ for four distinct times. The theoretical prediction given in Eq. (21) with an $a = 3.75 \times 10^{-8}$ is shown by the black line.

can observe that at the left we obtain the scale $\mu = 0.5$ and at the right we obtain $\mu = 0.65$. So, we have two distinct behaviors: at the left a normal diffusion and at the right we have a superdiffusive behavior.

The scaling hypothesis is carried forward using Eq. (20) to obtain $\phi^{2\mu} = a\sqrt{\pi}\langle \bar{x}(\phi)^2 \rangle / \Gamma(3/2)$, which enables us to specify the subsequent function

$$f_\phi(\xi) = \phi^\mu \Psi_\mu(\bar{x}, \phi) = \sqrt{\frac{a}{\pi}} \exp\left[-\frac{\Gamma(3/2)}{\sqrt{\pi}} \xi \right], \qquad (21)$$

where $\xi = \bar{x}^2/\langle \bar{x}(\phi)^2 \rangle$. Using the PDF data for the superdiffusive process ($\mu = 0.65$) we obtain $f_\phi(\xi)$ numerically and the results for $\phi = 0.76$, $\phi = 0.765$, $\phi = 0.89$, and $\phi = 0.995$ are presented in Fig. 8. The only parameter that can be adjusted in the theoretical forecast stated in Eq. (21) is the value of a. We get a remarkable agreement with the simulation findings when we choose $a = 3.75 \times 10^{-8}$. The black dot-dashed line on the graph denotes the theoretical result obtained in Eq. (21). We observe that the theoretical modeling and the simulation outcome start to diverge for periods of time less than 76.5% of the overall duration of the iterative procedure. Rescaling the data, all simulation points for times more than this amount lie exactly on the same curve. This was already a foregone conclusion if we look at the second PDF in Fig. 6, which shows quite anomalous behavior for times less than 0.8. Before this time has elapsed the particles display a strongly anomalous diffusion with a scale that must rely on the moment being estimated, $\langle |x|^m \rangle \propto t^{m\mu(m)}$ [20].

V. CONCLUSIONS AND OUTLOOK

In this work, we have studied a falling particle in the gravitational field colliding with a nonplane surface. We could observe that the horizontal component of the collision force presented a stochastic behavior. This was verified by using the entropy permutation method applied to the collision force time series. Additionally, we established that the jumps to the right and left follow a distribution whose probabilities tend toward 0.5 while the particle's temporal development takes place. It can be seen that the convergence to the factor 0.5 occurs significantly more quickly using the ground with parameters $\alpha = 0.01$ and $\beta = 0.005$ than with $\beta = 0.0005$. We assume that a surface with more pronounced undulations produces a horizontal component of the force that swiftly alters the particle's horizontal motion, causing the probability of jumps to fast converge to 0.5. The first case implied a diffusion process that follows Einstein's famous relationship so that the horizontal mean-squared displacement is proportional to time, $\langle x(t)^2 \rangle \sim t$. The system begins to become superdiffusive as the ground gets smoother. In fact, it is observed that the system with $\beta = 0.0005$ exhibits a strongly anomalous mean-squared deviation with temporal increase over the earliest portion of its temporal history. Subsequently, the movement becomes " standard superdiffusive." To comprehend this behavior, we assumed that the probability density's functional form must take on a Gaussian form of normal diffusion, with the exception that the distribution's time dependence is scaled by t^μ. We get a remarkable consistency between the theoretical expression and the simulation results using this approach. Future works are being developed including changes in the function that describes the floor, the introduction of dissipation, and oscillations in the ground, among other works.

ACKNOWLEDGMENTS

The authors would like to thank Edson Denis Leonel for the observations and comments, as well as Coordenação de Aperfeiçoamento de Pessoal de Nível Superior (Capes) for financial support.

APPENDIX: JACOBIAN MATRIX

The Jacobian matrix $J = \partial(F_1, F_2, F_3)/\partial(v_x, v_y, p)$ for this dynamical system may be simply calculated using Eqs. (11a)–(13), leading to

$$\frac{\partial F_1}{\partial v_x} = \frac{\bar{\alpha}^4 + 4\bar{\beta} {v_y}^2 \cos\left(p + \frac{2v_x v_y}{\bar{\alpha}}\right)\left[\bar{\alpha}^2 - \bar{\beta}^2 \sin^2\left(p + \frac{2v_x v_y}{\bar{\alpha}}\right)\right] - \bar{\beta}^4 \sin^4\left(p + \frac{2v_x v_y}{\bar{\alpha}}\right) - 4\bar{\alpha}\bar{\beta}^2 v_x v_y \sin\left(2p + \frac{4v_x v_y}{\bar{\alpha}}\right)}{\left[\bar{\alpha}^2 + \bar{\beta}^2 \sin^2\left(p + \frac{2v_x v_y}{\bar{\alpha}}\right)\right]^2},$$

$$\frac{\partial F_1}{\partial v_y} = \frac{2\bar{\beta}\left\{\bar{\alpha}\left[-2\bar{\beta} {v_x}^2 \sin\left(2p + \frac{4v_x v_y}{\bar{\alpha}}\right) + \bar{\alpha}^2 \sin\left(p + \frac{2v_x v_y}{\bar{\alpha}}\right) + \bar{\beta}^2 \sin^3\left(p + \frac{2v_x v_y}{\bar{\alpha}}\right)\right] + 2v_x v_y \cos\left(p + \frac{2v_x v_y}{\bar{\alpha}}\right)\left[\bar{\alpha}^2 - \bar{\beta}^2 \sin^2\left(p + \frac{2v_x v_y}{\bar{\alpha}}\right)\right]\right\}}{\left[\bar{\alpha}^2 + \bar{\beta}^2 \sin^2\left(p + \frac{2v_x v_y}{\bar{\alpha}}\right)\right]^2},$$

$$\frac{\partial F_1}{\partial p} = \frac{2\bar{\alpha}\bar{\beta}\cos\left(p + \frac{2v_x v_y}{\bar{\alpha}}\right)\left(\bar{\alpha}^2 v_y - \bar{\beta}\sin\left(p + \frac{2v_x v_y}{\bar{\alpha}}\right)\left[\bar{\beta} v_y \sin\left(p + \frac{2v_x v_y}{\bar{\alpha}}\right) + 2\bar{\alpha} v_x\right]\right]}{\left[\bar{\alpha}^2 + \bar{\beta}^2 \sin^2\left(p + \frac{2v_x v_y}{\bar{\alpha}}\right)\right]^2},$$

$$\frac{\partial F_2}{\partial v_x} = -\frac{2\bar{\beta}\{\bar{\alpha}[2\bar{\beta}{v_y}^2 \sin\left(2p+\frac{4v_xv_y}{\bar{\alpha}}\right)+\bar{\alpha}^2\sin\left(p+\frac{2v_xv_y}{\bar{\alpha}}\right)+\bar{\beta}^2\sin^3\left(p+\frac{2v_xv_y}{\bar{\alpha}}\right)]+2v_xv_y\cos\left(p+\frac{2v_xv_y}{\bar{\alpha}}\right)[\bar{\alpha}^2-\bar{\beta}^2\sin^2\left(p+\frac{2v_xv_y}{\bar{\alpha}}\right)]\}}{\left[\bar{\alpha}^2+\bar{\beta}^2\sin^2\left(p+\frac{2v_xv_y}{\bar{\alpha}}\right)\right]^2},$$

$$\frac{\partial F_2}{\partial v_y} = \frac{\bar{\alpha}^4-\bar{\beta}\{4{v_x}^2\cos\left(p+\frac{2v_xv_y}{\bar{\alpha}}\right)[\bar{\alpha}^2-\bar{\beta}^2\sin^2\left(p+\frac{2v_xv_y}{\bar{\alpha}}\right)]+\bar{\beta}^3\sin^4\left(p+\frac{2v_xv_y}{\bar{\alpha}}\right)+4\bar{\alpha}\bar{\beta}v_xv_y\sin\left(2p+\frac{4v_xv_y}{\bar{\alpha}}\right)\}}{\left[\bar{\alpha}^2+\bar{\beta}^2\sin^2\left(p+\frac{2v_xv_y}{\bar{\alpha}}\right)\right]^2},$$

$$\frac{\partial F_2}{\partial p} = -\frac{2\bar{\alpha}\bar{\beta}\cos\left(p+\frac{2v_xv_y}{\bar{\alpha}}\right)\{\bar{\beta}\sin\left(p+\frac{2v_xv_y}{\bar{\alpha}}\right)[2\bar{\alpha}v_y-\bar{\beta}v_x\sin\left(p+\frac{2v_xv_y}{\bar{\alpha}}\right)]+\bar{\alpha}^2v_x\}}{\left[\bar{\alpha}^2+\bar{\beta}^2\sin^2\left(p+\frac{2v_xv_y}{\bar{\alpha}}\right)\right]^2},$$

$$\frac{\partial F_3}{\partial v_x} = \frac{2v_y}{\bar{\alpha}},$$

$$\frac{\partial F_3}{\partial v_y} = \frac{2v_x}{\bar{\alpha}},$$

$$\frac{\partial F_3}{\partial p} = 1,$$

where we used an abbreviated notation (v_x, v_y, p) rather than $(\bar{v}_{x_n}^{(r)}, \bar{v}_{y_n}^{(r)}, p_n)$ to simplify the expressions. It is straightforward to show that the Jacobian matrix's determinant is equal to 1, confirming that the system is indeed conservative and the dimensionless energy

$$\bar{E}_n = \tfrac{1}{2}\left[\left(\bar{v}_{x_n}^{(r)}\right)^2 + \left(\bar{v}_{y_n}^{(r)}\right)^2\right] \tag{A1}$$

is constant.

[1] S. K. Ma, *Statistical Mechanics* (World Scientific, Singapore, 1985).
[2] J. G. Berryman, J. Math. Phys. **18**, 2108 (1977).
[3] M. F. Shlesinger, J. Klafter, and B. J. West, Phys. A (Amsterdam, Neth.) **140**, 212 (1986).
[4] X. Yu and D. M. Leitner, J. Chem. Phys. **119**, 12673 (2003).
[5] A. J. Lichtenberg and M. A. Lieberman, *Regular and Chaotic Dynamics* (Springer, New York, 1992).
[6] S. H. Strogatz, *Nonlinear Dynamics and Chaos with Student Solutions Manual* (CRC Press, Boca Raton, Florida, 2018).
[7] S. Strogatz, M. Friedman, A. J. Mallinckrodt, and S. McKay, Comput. Phys. **8**, 532 (1994).
[8] T. Geisel, J. Nierwetberg, and A. Zacherl, Phys. Rev. Lett. **54**, 616 (1985).
[9] J. Szymanski and M. Weiss, Phys. Rev. Lett. **103**, 038102 (2009).
[10] M. J. Saxton, Biophys. J. **81**, 2226 (2001).
[11] P. Massignan, C. Manzo, J. A. Torreno-Pina, M. F. Garcia-Parajo, M. Lewenstein, and G. J. Lapeyre, Phys. Rev. Lett. **112**, 150603 (2014).
[12] A. L. P. Livorati, T. Kroetz, C. P. Dettmann, I. L. Caldas, and E. D. Leonel, Phys. Rev. E **86**, 036203 (2012).
[13] T. Harayama and P. Gaspard, Phys. Rev. E **64**, 036215 (2001).
[14] E. D. Leonel, Marcus Vinícius Camillo Galia, L. A. Barreiro, and D. F. M. Oliveira, Phys. Rev. E **94**, 062211 (2016).
[15] Y. A. Kuznetsov, *Elements of Applied Bifurcation Theory* (Springer, New York, 1995).
[16] C. Bandt and B. Pompe, Phys. Rev. Lett. **88**, 174102 (2002).
[17] M. Riedl, A. Muller, and N. Wessel, Eur. Phys. J.: Spec. Top. **222**, 249 (2013).
[18] F. Cecconi, G. Costantini, A. Taloni, and A. Vulpiani, Phys. Rev. Res. **4**, 023192 (2022).
[19] B. B. Mandelbrot and J. W. V. Ness, SIAM Rev. **10**, 422 (1968).
[20] K. H. Andersen, P. Castiglione, A. Mazzino, and A. Vulpiani, Eur. Phys. J. B **18**, 447 (2000).